ISSN 1027-4510, Journal of Surface Investigation: X-ray, Synchrotron and Neutron Techniques, 2022, Vol. 16, No. 1, pp. 134–139. © Pleiades Publishing, Ltd., 2022.
Russian Text © The Author(s), 2022, published in Poverkhnost', 2022, No. 2, pp. 51–57.

Effect of Nanostructuring of the Surface of a Lead Sulfide Crystal in Plasma on the Optical Reflection Spectra

S. P. Zimin[a, b, *], N. N. Kolesnikov[c], M. S. Tivanov[d, **], L. S. Lyashenko[d], I. I. Amirov[a], V. V. Naumov[a], and E. S. Gorlachev[a]

[a] *Yaroslavl Branch, Valiev Institute of Physics and Technology, Russian Academy of Sciences, Yaroslavl, 150007 Russia*

[b] *Demidov State University, Yaroslavl, 150003 Russia*

[c] *Institute of Solid State Physics, Russian Academy of Sciences, Chernogolovka, 142432 Russia*

[d] *Department of Physics, Belarusian State University, Minsk, 220030 Belarus*

**e-mail: zimin@uniyar.ac.ru*

***e-mail: michael.tivanov@gmail.com*

Received May 25, 2021; revised July 26, 2021; accepted July 30, 2021

Abstract—A study of the optical-reflection spectra (250–2500 nm) for the surface of lead sulfide crystals in the initial state and after the formation of a homogeneous ensemble of nanostructures is conducted. Single crystals of PbS are grown using the vertical-zone-melting method, with the [100] orientation along the growth axis. Surface nanostructuring is realized in a reactor of high-density argon plasma with a low-pressure high-frequency inductive discharge (13.56 MHz) at the ion energy ~200 eV. The uniform array of stepped lead sulfide nanostructures formed due to plasma treatment is up to 140 nm in height, with cruciform bases having ⟨100⟩-oriented lateral orthogonal elements 20–60 nm long. It is found that the specular-reflection- and diffuse-reflection spectra for the initial surface of the (100) PbS crystals and for that nanostructured in argon plasma differ significantly. Using the Kubelka–Munk theory of diffuse reflection and the Kumar theory of specular reflection, the band-gap value for the nanostructured surface of (100) PbS crystals is determined as 3.45–3.47 eV, exceeding the value for the initial surface of lead sulfide ~0.4 eV.

Keywords: lead sulfide, ion-plasma treatment, nanostructures, optical-reflection spectra, quantum-confinement effects

DOI: 10.1134/S1027451022010384

INTRODUCTION

Lead sulfide, PbS, is one of the most promising materials in semiconductor-material science. Having a band gap value of 0.4 eV at 300 K, PbS is widely used for manufacturing IR detectors, gas sensors, thin-film transistors, photovoltaic elements, and the like [1–3]. Due to the low effective masses of charge carriers and high dielectric permeability in lead sulfide, the exciton Bohr radius is great (18 nm) enabling one to implement quantum-confinement effects in nanoparticles of rather large sizes. By means of dimensional quantization, the band-gap value of PbS may be increased up to 5.2 eV [4]. Over the last two decades great interest has been shown in the development of methods for the nanostructuring of PbS intended for applications in new facilities of alternative power generation, in thermoelectric systems, optoelectronic and nanoelectronic devices [5–8]. Among the various methods for nanostructuring lead chalcogenides, advantages have been exhibited by the methods used for ion-plasma treatment described in the review [9].

The objective of this work is to form an ensemble of nanostructures on the surface of single-crystal (100) PbS wafers by means of plasma treatment and to establish the optical characteristics of the nanostructured surface as compared with the initial single-crystal state.

EXPERIMENTAL

Single crystals of lead sulfide were grown by the vertical-zone-melting method in an atmosphere of argon at a pressure of 1.2 MPa and growth rate of 2 mm/h. The grown single crystals of PbS were [100]-oriented along the growth axis, with the chemical composition showing the slight prevalence of metal (S—49.05 at %, Pb—50.95 at %). An ingot was cleaved perpendicular to the growth axis into the wafers, the surface of which was mechanically polished with sub-

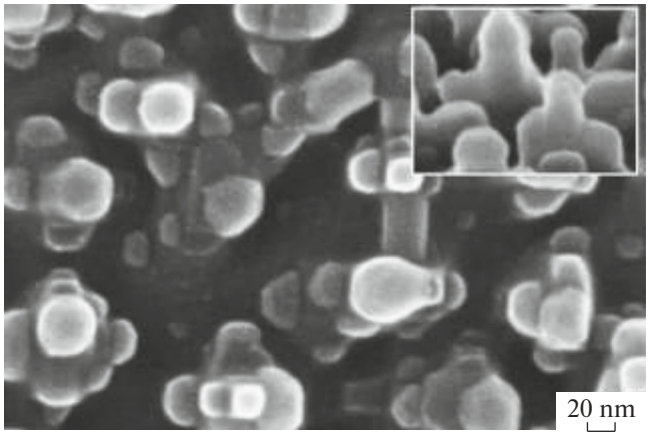

Fig. 1. SEM image of the surface of a (100) PbS crystal nanostructured in argon plasma. The inset shows the surface imaged at an angle of 70° on the same scale.

sequent chemical purification. The surface nanostructuring of the wafers was implemented in a reactor of high-density argon plasma with a low-pressure high-frequency inductive discharge (13.56 MHz) with the following treatment conditions: argon flow rate of 10 sccm, working pressure in the reactor of 0.07 Pa, RF inductor power of 800 W, and the RF bias power of the aluminum substrate holder of 200 W. The energy of Ar^+ ions was ~200 eV; plasma treatment was carried out in two sequential steps with a duration of 2 and 3 min.

The surface morphology was estimated by means of scanning electron microscopy (SEM) with the help of a Supra 40 (Carl Zeiss) unit in the secondary-electron recording mode (InLens detector). The Raman spectra were recorded by a Nanofinder HE (LOTIS TII) confocal spectrometer. Excitation was provided by a solid-state laser operating in the continuous mode at the wavelength 532 nm and optical power ~200 μW. Laser radiation was focused on the surface of the sample to a spot diameter of ~0.6 μm. The Raman spectra were recorded over the range 50–700 cm^{-1} at a spectral resolution of no worse than 3 cm^{-1}. The diffuse optical-reflection spectra were recorded by a Lambda 1050 UV/Vis/NiR (Perkin Elmer) spectrophotometer with the use of an integrating sphere, the specular optical-reflection spectra were recorded using Lambda 1050 UV/Vis/NiR (Perkin Elmer) and Photon RT (EssentOptics) spectrophotometers. The reflection spectra were recorded at a spectral resolution of no worse than 5 nm over the wavelength range 250–2500 nm in nonpolarized light. The beam size of optical radiation on the surface of the sample under study was about 5 × 5 mm.

RESULTS AND DISCUSSION

Figure 1 shows SEM images of an ensemble of stepped nanostructures with cruciform bases formed due to plasma treatment. At the tips of the nanostructural elements forming the second step at the center of the cruciform bases, quasi-spherical lead droplets are found. The total length of the nanostructures comes to 140 nm and the sizes of the lead droplets at the tip vary within the limits 25–70 nm. The lengths and heights of the lateral elements in the ⟨100⟩ directions are within the range 20–60 nm and the surface density of the nanostructures is 5×10^9 cm^{-2}.

Figure 2 presents the Raman spectra for the surface of (100) PbS crystals in the initial state and after nanostructuring in argon plasma. Deconvolution of the Raman spectra in the Lorentz approximation points to the presence of peaks characteristic for PbS, $PbO{\cdot}PbSO_4$, and PbO (Table 1) [10–17]. The Raman lines characteristic for PbS are observed both before and after ion-plasma treatment of the surface. For the peaks in the Raman spectra of PbS, plasma treatment leads to the greatest increase in the intensity of the line at 271/281 cm^{-1}, i.e., by a factor of 3.5, which, apart from the PbS phase [12], may be assigned to the phases $PbO{\cdot}PbSO_4$ [13] and PbO [14, 16].

An increase in the intensity of the line at 407 cm^{-1} was also observed in [11] when PbS powder was pulverized to a few tens of nanometers, whereas in [13, 14] this line was assigned to the phases $PbO{\cdot}PbSO_4$ or PbO. According to [17], the line observed after ion-plasma treatment at 533 cm^{-1} corresponds to nanocrystalline α-PbO. In this way, the data of Raman spectroscopy suggest that on the surface of PbS wafers nanostructured as a result of treatment in argon plasma during storage in air, the intensification of oxidation processes occurs with the formation of $PbO{\cdot}PbSO_4$ and PbO phases.

Spectral dependences of the specular and diffuse reflectance R for the initial surface of (100) PbS crystals and that nanostructured in argon plasma are given in Fig. 3. Both for the initial and nanostructured surface the specular reflectance is independent of the radiation incidence angle (from 8° to 64°) that is peculiar to a surface with the geometrical sizes of structural elements which are considerably less than the wavelength of incident light. Besides, the spectra of specular and diffuse reflection in the visible and IR ranges are coincident and a marked component of scattered radiation is observed only in the UV range.

The spectral-dependence curve for the specular reflectance of the initial crystalline surface has a distinct wide peak at 365 nm (3.4 eV) and a less pronounced peak at 690 nm (1.8 eV), with the reflectance 46 and 41% at the maximum, respectively. According

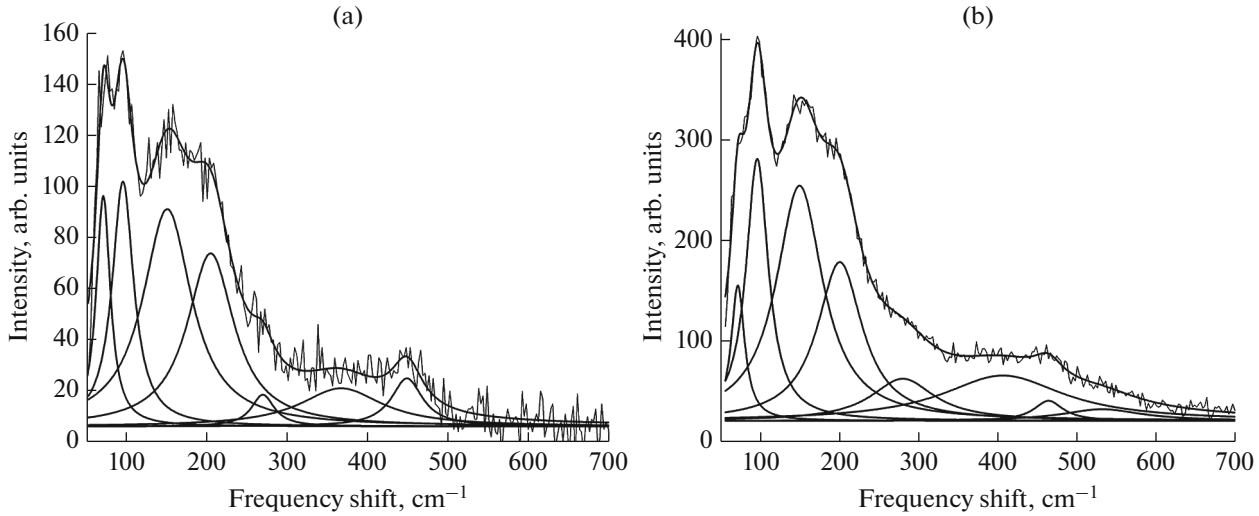

Fig. 2. Raman spectra of the initial surface of (100) PbS crystals (a) and of that nanostructured in argon plasma (b).

to their energy positions, the indicated peaks correspond to the well-known experimentally observed peaks E_1 and E_2 of lead sulfide in terms of the reflection spectra and to the energy gaps for allowed vertical electronic transitions at the degenerate point L of the Brillouin zone [18, 19]. In the 900–2500 nm region, the reflectance changes insignificantly, amounting to ~39%.

Nanostructuring of the surface of (100) PbS crystals leads to significant changes in the spectra of specular and diffuse reflection (Fig. 3): the peaks E_1 and E_2 characteristic for the reflection spectra of PbS disappear; the specular and diffuse reflectance decrease in the entire investigated range. For diffuse reflection, the Kubelka–Munk function [20]:

$$F(R) = \frac{(1-R)^2}{2R},$$

is proportional to the absorption coefficient, enabling one to determine the band-gap value E_g from the linear part of the dependence $(F(R)h\nu)^2$ on the photon energy $h\nu$ for a direct-gap semiconductor material [21, 22]. The value of E_g for the initial surface of (100) PbS crystals, derived with the use of the Kubelka–Munk function in Tauc coordinates, equals ~0.4 eV (Fig. 4) in line with the known value of E_g for bulk PbS [23,

Table 1. Observed Raman lines for the initial surface of (100) PbS crystals and for that nanostructured in the argon plasma: *P* is the line position, *FWHM* is the full width at half maximum, *I* is the intensity

Observed lines						Published data		
Initial surface			Surface nanostructured in argon plasma			PbS [10–12]	$PbO{\cdot}PbSO_4$ [13, 14]	PbO [15–17]
P, cm^{-1}	*FWHM*, cm^{-1}	I, arb. units	P, cm^{-1}	*FWHM*, cm^{-1}	I, arb. units	P, cm^{-1}	P, cm^{-1}	P, cm^{-1}
73	22	90	73	21	135	–	–	71
97	32	96	98	34	260	96	–	–
152	74	85	151	72	233	151/156	–	–
206	71	68	202	69	157	205	–	–
271	34	12	281	97	42	287	285	282/286
368	124	15	–	–	–	384	–	–
–	–	–	407	186	45	420	427	–
450	47	19	465	45	20	456/462/476	–	–
–	–	–	533	122	12	–	–	530

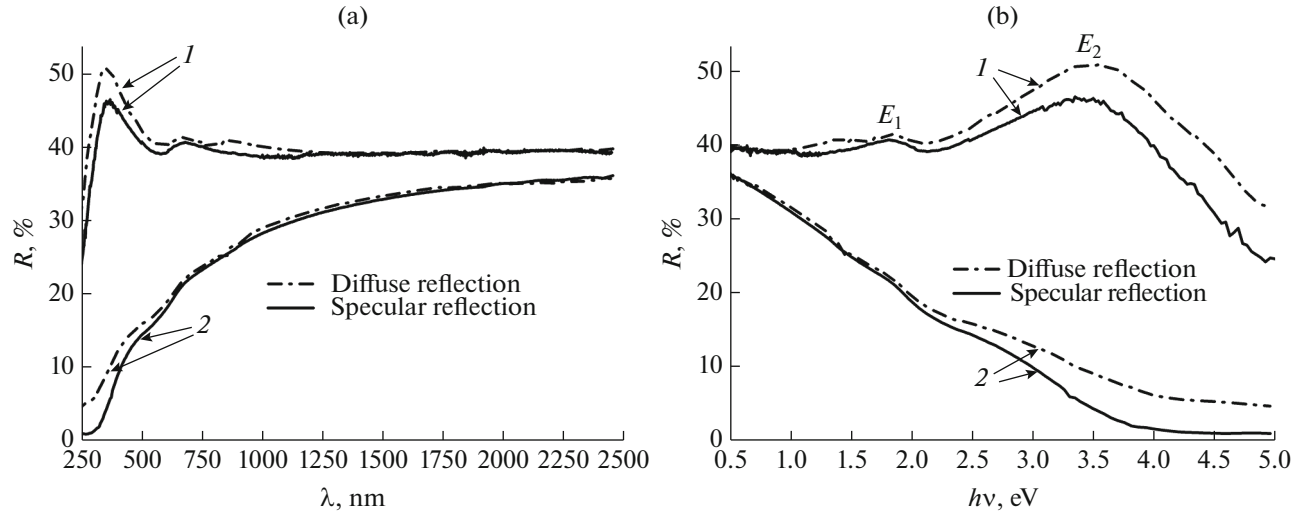

Fig. 3. Spectra of specular (8°) and diffuse reflection for the surface of (100) PbS crystals on the scale of wavelengths (a) and energies (b): *1* initial, *2* nanostructured in the argon plasma.

24]. The energies of the electronic transitions E_1 and E_2 at the point L of the Brillouin zone are associated with two critical points of the curve $(F(R)h\nu)^2$ (Fig. 4).

The value of E_g for the surface of (100) PbS crystal nanostructured in argon plasma, determined in a similar way from the spectrum of diffuse reflection in accordance with the Kubelka–Munk theory (Fig. 5a), is equal to 3.45 eV, and exceeds considerably the value for the initial surface. To find E_g from the specular-reflection spectrum for the nanostructured surface of PbS, let us use Kumar theory [25, 26] as the reflection spectrum in this case is close to a "stepped" form [27, 28]. The value of E_g, derived from the specular-reflection spectrum according to a linear part of the dependence:

$$\left[h\nu \ln\left(\frac{R_{max} - R_{min}}{R - R_{min}}\right)\right]^2,$$

on $h\nu$ in the assumption of direct-gap transitions, is 3.47 eV (Fig. 5b), supporting the result obtained from the diffuse-reflection spectrum. In such a manner the value $E_g \sim 3.45–3.47$ eV, derived from the spectra of specular and diffuse reflection for the surface of (100) PbS crystals nanostructured in argon plasma, exceeds considerably the value of E_g for bulk PbS. Similar values of E_g for nanocrystals of PbS, 10–15 nm in size, were obtained in [24]: 3.36 eV, and for PbS nanoparticles, with sizes below 10 nm, in [29]: 3.35 eV.

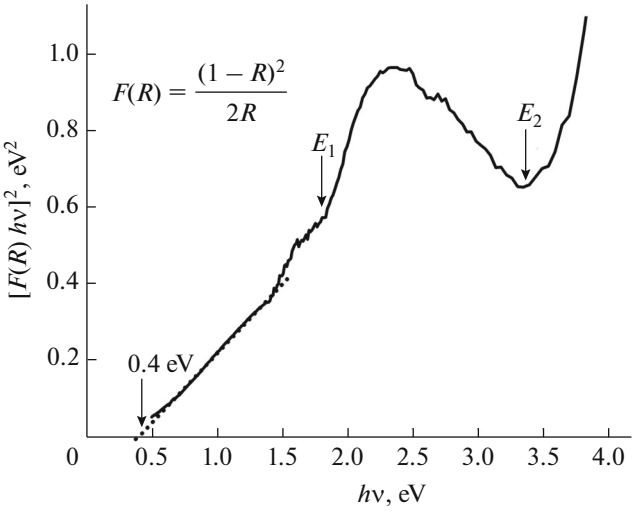

Fig. 4. Kubelka–Munk function of diffuse reflection for the initial surface of (100) PbS crystals on Tauc coordinates.

The observed significant increase in the band-gap value up to $E_g \sim 3.45–3.47$ eV for the surface of (100) PbS crystals, representing an ensemble of stepped complex nanostructures having orthogonally oriented cruciform bases with elements 20–60 nm in size, may be related to the quantum-confinement effect [4]. As, according to publications, close values of E_g are observed for nanostructures of PbS with considerably smaller sizes [4, 24, 29], on the basis of the obtained Raman spectroscopy data, it is suggested that, after plasma treatment of the surface of (100) PbS crystals, nanostructures of PbS covered by a $PbO{\cdot}PbSO_4/PbO$ shell are formed when extracted into an air atmosphere. The formation of an oxide shell results in the fact that the effective size of the PbS nanostructures is smaller than that observed with the help of SEM and is less than the exciton Bohr radius, leading to the

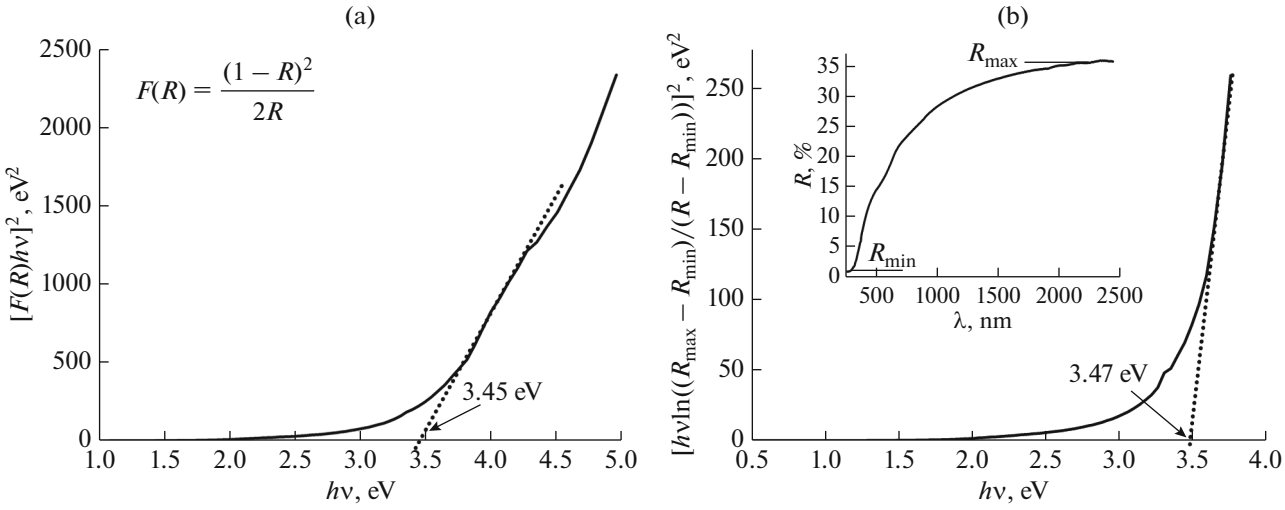

Fig. 5. Kubelka–Munk function of diffuse reflection (a) and the Kumar function of specular reflection (b) for the surface of (100) PbS crystals nanostructured in argon plasma on Tauc coordinates.

quantum-confinement effect for relatively thick nanostructures [30].

In the region of the absorption edge, the Kubelka–Munk function obeys the Urbach rule (Fig. 6), i.e., the absorption coefficient of the nanostructured surface grows exponentially as the energy of the incident photon grows. This points to some structural imperfection of the formed nanostructures (the presence of Urbach's "tail") but, due to the low value of the Urbach energy (~0.26 eV), it is believed that the ensemble of nanostructures on the surface is rather homogeneous.

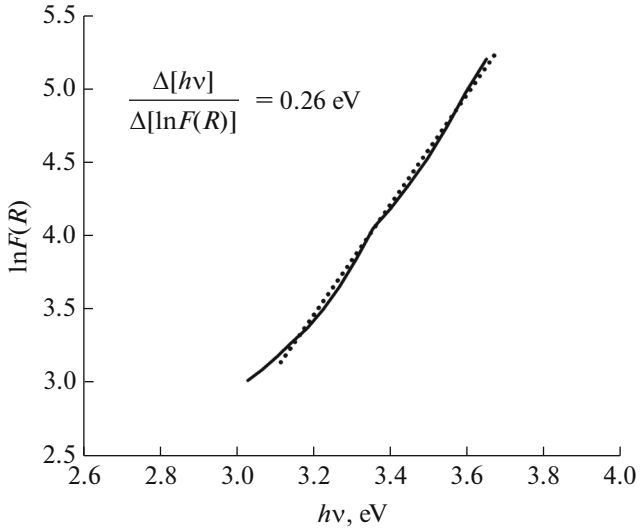

Fig. 6. Curve of $\ln F(R)$ as a function of the photon energy $h\nu$ for the surface of (100) PbS crystals nanostructured in argon plasma.

CONCLUSIONS

As shown by the results of the study performed, argon-plasma treatment of the surface of (100) PbS crystals results in the formation of a uniform array of stepped lead sulfide nanostructures with cruciform bases. The data of Raman spectroscopy point to the fact that, after plasma treatment and subsequent storage in air, intensive oxidation processes of the nanostructured surface with the formation of $PbO{\cdot}PbSO_4$ and PbO phases take place. It has been found that the specular and diffuse reflection spectra of the initial surface of (100) PbS crystals and of that nanostructured in argon plasma differ considerably. Using the Kubelka–Munk theory of diffuse reflection and the Kumar theory of specular reflection, the band-gap value has been determined for the nanostructured surface of (100) PbS crystals as 3.45–3.47 eV. The obtained value of the band gap exceeding that for the initial surface of lead sulfide ~0.4 eV may be due to confinement effects in lead sulfide for a system comprising "PbS nanoparticles + oxide shell".

FUNDING

The work was performed within the State assignment of the RF Ministry of Science and Higher Education for the Valiev Institute of Physics and Technology, Russian Academy of Sciences, program no. 0066-2019-0002; the State assignment of the RF Ministry of Science and Higher Education for the Institute of Solid State Physics, Russian Academy of Sciences; initiative research of Yaroslavl State University, and State Research Program of the Republic of Belarus "Material Science, Innovative Materials and Technologies."

CONFLICT OF INTEREST

We declare that we have no conflicts of interest.

REFERENCES

1. Yu. I. Ravich, B. A. Efimova, and I. A. Smirnov, *Methods to Study of Semiconductors as Applied to Lead Chalcogenides PbTe, PbSe, PbS* (Nauka, Moscow, 1968) [in Russian].
2. T. Fu, Sens. Actuators, B **140**, 116 (2009). https://doi.org/10.1016/j.snb.2009.03.075
3. A. Carrillo-Castillo, A. Salas-Villasenor, I. Mejia, S. Aguirre-Tostado, B. E. Gnade, and M. A. Quevedo-López, Thin Solid Films **520**, 3107 (2012). https://doi.org/10.1016/j.tsf.2011.12.016
4. R. Thielsch, T. Böhme, R. Reiche, D. Schläfer, H.-D. Bauer, and H. Böttcher, Nanostruct. Mater. **10**, 131 (1998). https://doi.org/10.1016/S0965-9773(98)00056-7
5. T. Blachowicz and A. Ehrmann, Appl. Sci. **10**, 1743 (2020). https://doi.org/10.3390/app10051743
6. N. Sukharevska, D. Bederak, V. M. Goossens, J. Momand, H. Duim, D. N. Dirin, M. V. Kovalenko, B. J. Kooi, and M. A. Loi, ACS Appl. Mater. Interfaces **13**, 5195 (2021). https://doi.org/10.1021/acsami.0c18204
7. M. Ibáñez, Z. Luo, A. Genç, L. Piveteau, S. Ortega, D. Cadavid, O. Dobrozhan, Y. Liu, M. Nachtegaal, M. Zebarjadi, J. Arbiol, M. V. Kovalenko, and A. Cabot, Nat. Commun. **7**, 10766 (2016). https://doi.org/10.1038/ncomms10766
8. X. Zhang, Y. Chen, L. Lian, Z. Zhang, Y. Liu, L. Song, C. Geng, J. Zhang, and S. Xu, Nano Res. **14**, 628 (2021). https://doi.org/10.1007/s12274-020-3081-5
9. S. Zimin, E. Gorlachev, and I. Amirov, "Inductively coupled plasma sputtering: Structure of IV–VI semiconductors," in *Encyclopedia of Plasma Technology*, Ed. by J. Leon Shohet (Taylor and Francis, New York, 2017).
10. P. Yin, R. Zhang, Y. Zhang, and L. Guo, Int. J. Mod. Phys. B **24**, 3257 (2010). https://doi.org/10.1142/s0217979210066422
11. A. V. Baranov, K. V. Bogdanov, E. V. Ushakova, S. A. Cherevkov, A. V. Fedorov, and S. Tscharntke, Opt. Spectrosc. **109**, 268 (2010). https://doi.org/10.1134/s0030400x10080199
12. K. S. Upadhyaya, M. Yadav, and G. K. Upadhyaya, Phys. Status Solidi B **229**, 1129 (2002). https://doi.org/10.1002/1521-3951(200202)229:3<1129:aid-pssb1129>3.0.co;2-6
13. Y. Batonneau, C. Bremard, J. Laureyns, and J. C. Merlin, J. Raman Spectrosc. **31**, 1113 (2000). https://doi.org/10.1002/1097-4555(200012)31:12<1113:aid-jrs653>3.0.co;2-e
14. G. De Giudici, P. Ricci, P. Lattanzi, and A. Anedda, Am. Mineral. **92**, 518 (2007). https://doi.org/10.2138/am.2007.2181
15. O. Semeniuk, A. Csik, S. Kokenyesi, and A. Reznik, J. Mater. Sci. **52**, 7937 (2017). https://doi.org/10.1007/s10853-017-0998-5
16. H. Miyagawa, D. Kamiya, C. Sato, and K. Ikegami, J. Mater. Sci. **34**, 105 (1999). https://doi.org/10.1023/a:1004421826443
17. M. Cortez-Valadez, A. Vargas-Ortiz, L. Rojas-Blanco, H. Arizpe-Chávez, M. Flores-Acosta, and R. Ramírez-Bon, Phys. E (Amsterdam, Neth.) **53**, 146 (2013). https://doi.org/10.1016/j.physe.2013.05.006
18. M. Cardona and D. L. Greenaway, Phys. Rev. A **133**, A1685 (1964). https://doi.org/10.1103/physrev.133.a1685
19. S. E. Kohn, P. Y. Yu, Y. Petroff, Y. R. Shen, Y. Tsang, and M. L. Cohen, Phys. Rev. B **8**, 1477 (1973). https://doi.org/10.1103/PhysRevB.8.1477
20. P. Kubelka, J. Opt. Soc. Am. **38**, 448 (1948). https://doi.org/10.1364/josa.38.000448
21. K. Ullah, Z.-D. Meng, S. Ye, L. Zhu, and W.-C. Oh, J. Ind. Eng. Chem. **20**, 1035 (2014). https://doi.org/10.1016/j.jiec.2013.06.040
22. A. V. Stanchik, V. F. Gremenok, R. Juskenas, I. I. Tyukhov, M. S. Tivanov, Ch. Fettkenhauer, V. V. Shvartsman, R. Giraitis, U. Hagemann, and D. C. Lupascu, Sol. Energy **178**, 142 (2019). https://doi.org/10.1016/j.solener.2018.12.025
23. K. K. Nanda, F. E. Kruis, H. Fissan, and M. Acet, J. Appl. Phys. **91**, 2315 (2002). https://doi.org/10.1063/1.1431429
24. Z. Q. Mamiyev and N. O. Balayeva, Opt. Mater. **46**, 522 (2015). https://doi.org/10.1016/j.optmat.2015.05.017
25. V. Kumar, S. Kr. Sharma, T. Sharma, and V. Singh, Opt. Mater. **12**, 115 (1999). https://doi.org/10.1016/s0925-3467(98)00052-4
26. J. Vipin Kumar, M. K. Gaur, and T. P. Sharma, J. Optoelectron. Biomed. Mater. **1**, 52 (2009).
27. S. K. Sharma, L. Kumar, and T. P. Sharma, Chalcogenide Lett. **5** (4), 73 (2008).
28. M. Tivanov, I. Kaputskaya, A. Patryn, A. Saad, L. Survilo, and E. Ostretsov, Electr. Rev. **92** (9), 88 (2016). https://doi.org/10.15199/48.2016.09.23
29. B. G. Zaragoza-Palacios, A. R. Torres-Duarte, and S. J. Castillo, Res. Square **1**, 1 (2021). https://doi.org/10.21203/rs.3.rs-271679/v1
30. H. Jung, R. Kuljic, M. A. Stroscio, and M. Dutta, Appl. Phys. Lett. **96**, 153106 (2010). https://doi.org/10.1063/1.3400215